From seasonal flood pulse to seiche: Multi-frequency water-level fluctuations in a large shallow tropical lagoon (Nokoué Lagoon, Benin)

Alexis Chaigneau, Olaègbè Victor Okpeitcha, Yves Morel, Thomas Stieglitz, Arnaud Assogba, Morgane Benoist, Pierre Allamel, Jules Honfo, Thierry Derol Awoulmbang Sakpak, Fabien Rétif, et al.

▶ **To cite this version:**

Alexis Chaigneau, Olaègbè Victor Okpeitcha, Yves Morel, Thomas Stieglitz, Arnaud Assogba, et al.. From seasonal flood pulse to seiche: Multi-frequency water-level fluctuations in a large shallow tropical lagoon (Nokoué Lagoon, Benin). Estuarine, Coastal and Shelf Science, 2022, 267, pp.107767. 10.1016/j.ecss.2022.107767 . ird-03558970

HAL Id: ird-03558970
https://ird.hal.science/ird-03558970

Submitted on 22 Jul 2024

HAL is a multi-disciplinary open access archive for the deposit and dissemination of scientific research documents, whether they are published or not. The documents may come from teaching and research institutions in France or abroad, or from public or private research centers.

L'archive ouverte pluridisciplinaire **HAL**, est destinée au dépôt et à la diffusion de documents scientifiques de niveau recherche, publiés ou non, émanant des établissements d'enseignement et de recherche français ou étrangers, des laboratoires publics ou privés.

Distributed under a Creative Commons Attribution - NonCommercial 4.0 International License

Version of Record: https://www.sciencedirect.com/science/article/pii/S0272771422000270
Manuscript_e441740df95fc214f06df29103bb8cef

From seasonal flood pulse to seiche: Multi-frequency water-level fluctuations in a large shallow tropical lagoon (Nokoué Lagoon, Benin).

Alexis CHAIGNEAU[a,b,c,*], Victor OKPEITCHA[d,c,b], Yves MOREL[a], Thomas STIEGLITZ[e], Arnaud ASSOGBA[b], Morgane BENOIST[a,b], Pierre ALLAMEL[f], Jules HONFO[c], Thierry Derol AWOULMBANG SAKPAK[g], Fabien RÉTIF[h], Thomas DUHAUT[a], Christophe PEUGEOT[i], Zacharie SOHOU[b]

[a] Laboratoire d'Études en Géophysique et Océanographie Spatiale (LEGOS), Université de Toulouse, CNES, CNRS, IRD, UPS, Toulouse, France
[b] Institut de Recherches Halieutiques et Océanologiques du Bénin (IRHOB), Cotonou, Bénin,
[c] International Chair in Mathematical Physics and Applications (ICMPA–UNESCO Chair), University of Abomey-Calavi, Cotonou, Benin
[d] Laboratoire d'Hydrologie Appliquée (LHA), Institut National de l'Eau (INE), African Centre of Excellence for Water and Sanitation (C2EA), Université d'Abomey Calavi, Bénin
[e] Aix-Marseille Université, CNRS, IRD, INRAE, Coll France, CEREGE, Aix-en-Provence, France
[f] STATMarine, La Seyne Sur Mer, France
[g] Laboratoire des Technologies et Sciences Appliquées, Université de Douala, Douala, Cameroun
[h] RETIF FABIEN PHILIAN, Montferrier sur Lez, France
[i] Hydrosciences Montpellier (HSM), IRD, Univ. Montpellier, CNRS, IMT, Montpellier, France

[*]Corresponding Author: alexis.chaigneau@ird.fr

© 2022 published by Elsevier. This manuscript is made available under the CC BY NC user license
https://creativecommons.org/licenses/by-nc/4.0/

Abstract

This study investigated the main water-level (WL) variability modes of Nokoué Lagoon in Benin (West-Africa). The average WL ranges between 1.3 and 2.3 m between the low- and high-water seasons. Seasonal as well as weak interannual variations between 2018 and 2019 are driven by rainfall regime over the catchment and associated river inflow. At sub-monthly scales, the lagoon is tidally choked: ocean tides can reach 90 cm, whereas in the lagoon semi-diurnal and diurnal tides hardly reach few centimeters. Choking conditions vary with river inflow and ocean tide amplitude, correctly represented by a simple tidal choking model. Diurnal modulation and asymmetry of the tide are stronger (weaker) during high (low) water period. We also observed WL variations of ±5-10 cm at a fortnightly frequency, stronger during wet (high-water) season. Superimposed on the seasonal, fortnightly and tidal WL variations, we further observed short-term high-frequency seiche events. Mostly observed during dry (low-water) conditions, they are characterized by typical standing-wave oscillations of 5-10 cm amplitudes and 3 h periods. They are forced by the passage of fast-moving squall-lines that induce strong wind variations, heavy rainfalls and rapid drop-off of the air temperature. Results obtained in this study provide useful metrics for the validation of flood forecasting models to be implemented in Benin, and elsewhere on the West African coastline.

Keywords: Water-levels; Lagoons; Tides; Seiches; Nokoué; Wavelet analysis.

1. Introduction

In the eastern tropical Atlantic Ocean, the coastal zone bordering the Gulf of Guinea include a series of coastal lagoons of varying sizes (Allersma and Tilmans, 1993; Lalèyè et al., 2007; Adite and Winemiller, 1997; Adite et al., 2013). These lagoons are often the main mixing zone of continental freshwater and coastal seawater, supporting some of the most productive aquatic ecosystems in the world (Knoppers, 1994; Valiela, 1995; Duck and da Silva, 2012). These coastal systems support important ecosystem services for the local populations who benefit from these natural or semi-natural areas through different activities (fishing, tourism, sand and/or salt extraction, etc.) (Djihouessi et al., 2017; Newton et al., 2018).

Among the various Beninese coastal lagoons, Nokoué Lagoon (Figure 1) is the largest and most exploited of the country's water bodies (Lalèyè et al., 1995; 2003). This lagoon, which is also one of the most productive in West Africa (Lalèyè et al., 2007), is at the heart of important ecological and socio-economic issues. It is part of the RAMSAR site #1018, recognized to be of international importance for its various ecosystems that include flood plains, mangroves, floating vegetation, and diverse fauna. This lagoon also hosts several lacustrine villages inhabited by more than 60000 people living in stilt dwellings (Principaud, 1995). These local populations depend on this water body not only for fishing, which provides ~15000 tons of fish per year (Principaud, 1995), but also for domestic water supply, agriculture, market gardening, animal husbandry, etc. But the Nokoué Lagoon, also bordered by 3 major urban centers (Cotonou, Abomey-Calavi, and Sémè Podji) totalizing more than 1.5 million inhabitants, is strongly impacted by various anthropogenic pollution sources. For instance, the lagoon is the receptacle of numerous urban drains and direct discharge by the surrounding populations of various wastes which has led to a deterioration of the water quality (Adjahouinou et al., 2012; 2014; Aina et al., 2012a; 2012b). In addition, Nokoué Lagoon is also embedded within the 500 km long West African coastal water corridor that stretches from Lagos (Nigeria) to Accra (Ghana). This coastal corridor is projected to become the largest African urbanized area (Choplin, 2019), a development that will threaten the lagoons' ecosystems and their service function. The planning and implementation of coastal management strategies requires a comprehensive knowledge of processes involved in the physical, chemical and ecological dynamics of the Nokoué Lagoon.

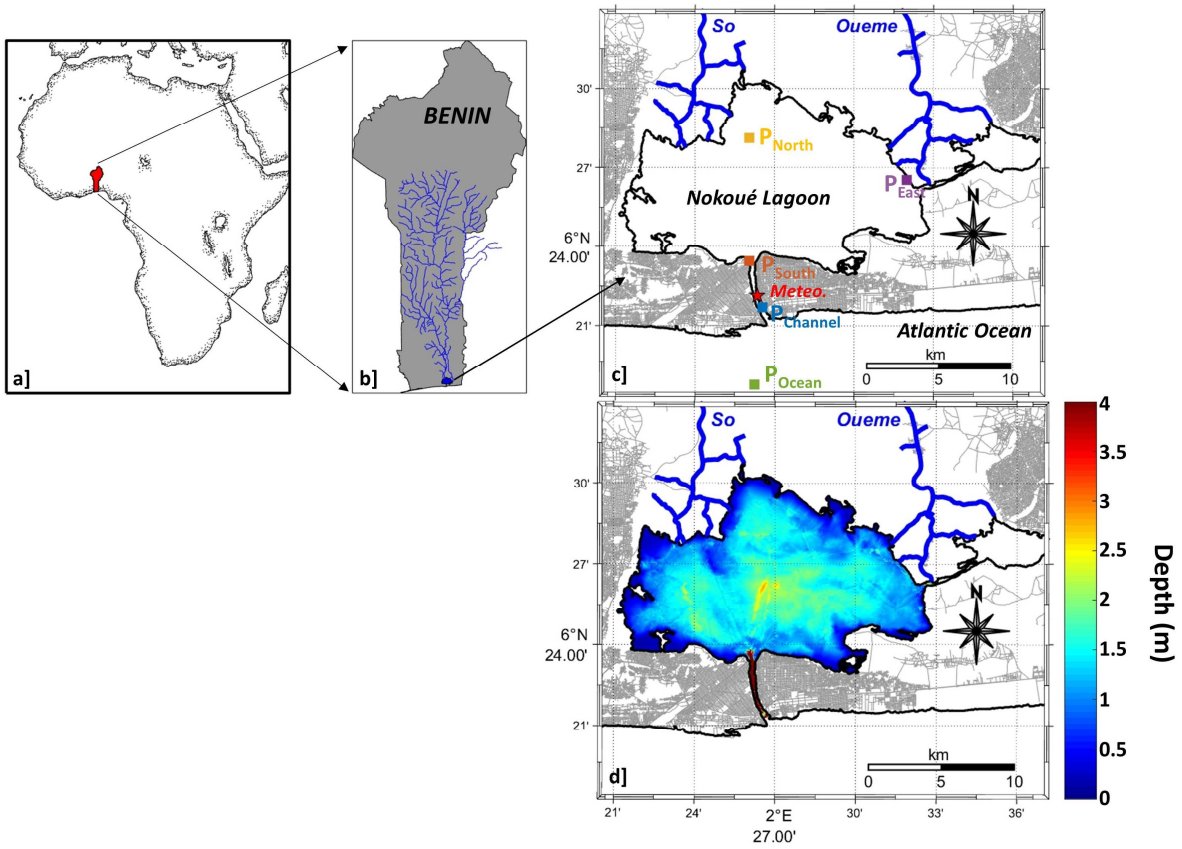

Figure 1. Geographical location of the Nokoué Lagoon in Benin. b] Hydrological network of the Sô and Ouémé river catchment basins. c] Position of the water-level stations (colored squares) and the weather station (red star). d] Bathymetry in low water season obtained from a spatial interpolation of ~123000 depth soundings.

One of the key parameters of coastal lagoon dynamics is the water level (WL) whose variations are mainly subject to the triple influence of (i) ocean tides, (ii) the hydrological variability of the catchment and (iii) direct rainfall contributions. Generally, high WL is associated with strong freshwater river discharge and low WL with time periods when salty oceanic water penetrates into the lagoon. First, WL fluctuations impact the lagoon circulation and consequently the turnover, residence or flushing times and therefore the dispersion or retention of pollutants. Second, the lagoon WL determines the exchange of properties between the continent and the ocean and controls the ecosystems by various direct or indirect processes. In a direct way, WL fluctuations control the salinity of the lagoon (e.g. Djihouessi and Aina, 2018), which directly impacts the ecosystem composition from plankton to fish (Le Barbé et al., 1993; Gnohossou, 2006; Adandedjan et al., 2017; Odountan et al., 2019; Laléyè et al., 2003; 2005). In an indirect way, WL variations impact lagoon and sediment dynamics by modifying erosion and sedimentation zones and the rate of sediment resuspension. Thus, turbidity and the availability of light on the vertical can vary according to the WL, which can modify the structure of biological communities, particularly phytoplankton

(Evtimova and Donohue, 2016). Similarly, WL fluctuations are correlated with modifications of nutrient concentrations, mixing and vertical stratification in the water column, eventually affecting the development, distribution and dilution of organisms as observed in other water bodies (e.g. Lobo et al., 2018; Stević et al., 2013).

Third, in addition to having direct or indirect effects on the ecosystem, variations in the WL of Nokoué Lagoon can have dramatic repercussions on local populations. Indeed, lacustrine villages and urbanized areas adjacent to the lagoon episodically experience flooding linked to major watershed floods and the regular overflow of the lagoon. For instance, in 2010, flooding killed tens of people and affected 360 000, leaving 100 000 homeless (World Bank, 2011; Ahouangan et al., 2014; Biao, 2017). More recently, in October-November 2019, the floods, less intense but spread over several weeks, also caused extensive damage and affected tens of thousands of households.

Finally, variations in the WL may also impact the quality of the groundwater that is exploited by residents bordering the lagoon, who use this unregulated shallow groundwater resource for domestic purposes, including drinking water supplies (Houéménou et al., 2020).

Despite the importance of monitoring and understanding WL fluctuations in particular to implement appropriate water resource and flood management measures, very few studies have described their variations in Nokoué Lagoon. On seasonal scales, Le Barbé et al. (1993) observed an increase of ~50-70 cm during the 1980 flood season. Similarly, using monthly observations acquired from 2001 to 2010, Djihouessi and Aina (2018) described an average seasonal WL variation of 55 cm. On (semi)diurnal scales, a hydrodynamic model calibrated with high-frequency WL measurements acquired over two 5-day periods, elucidated the tidal characteristics in the lagoon (Zandagba et al. 2016). Their simulation suggested a 2-4h phase shift between tidal fluctuations in the ocean and lagoon, and semi-diurnal tidal amplitudes of few centimeters in the lagoon. These 3 studies were based on limited observations obtained either over isolated and short time periods (Le Barbé et al., 1983; Zandagba et al., 2016), or at low temporal resolution (Djihouessi and Aina, 2018). Our study aims to fill this gap and to investigate WL variations in Nokoué lagoon at a wide range of time scales from a 2-year in-situ dataset at high temporal resolution (20 min sample intervals), and to determine the main physical mechanisms governing the observed fluctuations. Thanks to these intensive measurements, unique in West Africa, we complement past studies by

highlighting the different modes of WL variability to which Nokoué lagoon is subjected, from hourly to seasonal scales. We further aim at better characterizing the lagoon's tide, not only at the semi-diurnal scale as in Zandagba et al. (2016) but also at the diurnal scale and, in particular, investigating its asymmetry. Finally, various lagoons around the world are subject to wind-forced seiche phenomena (e.g. Chapman and Giese, 2001). Given the significant changes in the wind regime in Cotonou, especially during the passage of squall lines frequently observed in West Africa (Omotosho, 1984; 1985), it is likely that these seiche phenomena are also observed in the lagoon. In this study, we will therefore perform a wavelet analysis of the WL variations to highlight the different modes of variability, and will specifically describe the processes in the most energetic spectral bands.

2. Material and methods

2.1. Study area and hydrology

Nokoué is a coastal lagoon that extends about 20 km from east to west along the coast and 11 km from south to north (Figure 1), covering an average area of ~170 km^2 (Texier et al., 1980; Le Barbé et al., 1993; Mama et al., 2011; Djihouessi et al., 2019). Two main rivers flow into the lagoon on its northern shore, the Sô river, draining a relatively small catchment area of ~1000 km^2, and the Ouémé river, the largest Beninese river, which drains a catchment area of ~50000 km^2 (Le Barbé et al., 1993; Djihouessi et al., 2017). The Sô and the lower Ouémé valley flow into the Nokoué Lagoon forming a large flooded deltaic plain (e.g. Le Barbé et al., 1993). A third river, the Djonou, whose extension and flow are much smaller, also contributes to the freshwater inflow in the lagoon's southwestern part (Djihouessi and Aina, 2018).

On its southern part, Nokoué Lagoon is connected with the Atlantic Ocean by the ~280 m wide and ~4 km long Cotonou channel (Texier et al., 1980; Le Barbé et al., 1993). Through this relatively narrow channel, exchanges of fresh and salt water take place at the rhythm of the tides and the hydrological regime. Since the channel's construction in 1885, the previously unconnected 'Lake' Nokoué (as it is still known in colloquial language) is today an extensive lagoon that exhibits important salinity variations (e.g. Okpeitcha et al., 2022).

On the eastern side, Nokoué Lagoon is connected to the Porto-Novo lagoon (35 km^2) via the ~4 km long Totchè channel. Porto-Novo lagoon extends eastward into a

narrow coastal channel that discharges in the Atlantic Ocean at Lagos (Nigeria) at a distance of ~100 km from Nokoué Lagoon, with little effect on the dynamics and WL of Nokoué Lagoon (Texier et al., 1980; Le Barbé et al., 1993).

On seasonal scales, the lagoon's hydrological regime is driven by the West African summer monsoon related to the meridional shift of the intertropical convergence zone (ITCZ) and the associated intense tropical rain belt (Sultan and Janicot, 2000; Gu and Adler, 2004), resulting in two rainy and two dry seasons. The main rainy season extends from April-May to late July when the ITCZ moves northward from its near-equatorial southernmost position, while the second shorter and less intense rainy period extends from late September to November when the ITCZ migrates southward from its northernmost position (e.g. N'Tcha M'Po et al., 2017; Ahokpossi, 2018). However, this double rainy season and associated local rainfalls only slightly influence the WL of the Nokoué Lagoon that is more subject to the hydrology of the central part of Benin, where the main area of the Ouémé catchment takes place (e.g. Colleuil, 1987; see also Figure 1b). This latter region is characterized by a single rainy season, with maximum precipitation between July and October (Biao, 2017; Ahokpossi, 2018; Lawin et al., 2019, Colleuil, 1987). The maximum discharge into the lagoon between September and November is unknown (rivers ungauged in the coastal region) and varies, depending on authors, from ~400 $m^3\ s^{-1}$ (Le Barbé et al., 1993; Djihouessi and Aina, 2018) to more than 1000 $m^3\ s^{-1}$ (Lawin et al., 2019). This river discharge produces a complete desalinization of the Nokoué Lagoon and a strong increase of its volume (Texier et al., 1980; Colleuil, 1987; Djihouessi and Aina, 2018).

Figure 1d shows the bathymetry of the Nokoué Lagoon corresponding to the mean WL observed during low-water season in March-April. It was constructed using ~123000 depth soundings recorded with a Garmin GPSmap 421S echosounder and corrected for tidal and seasonal fluctuations. The mean and maximum depth is 1.3 m and 2.9 m, respectively. The lagoon deepens towards the Cotonou channel where the mean and maximum depths increase to ~3 m and ~8 m, respectively (Figure 1d).

2.2. Water level and atmospheric data

WL data was acquired by 4 pressure sensors deployed in the Cotonou channel and Nokoué Lagoon for a 2-year period (Figure 1c). Three of them ($P_{Channel}$, P_{South}, P_{North}) were located along a South-North axis whereas the 4th sensor (P_{East}) was deployed East

of the lagoon. More precisely, $P_{Channel}$ is located at 1.5 km from the coastal ocean; P_{South} is located at the lagoon entrance; P_{North} is located 8.5 km North of P_{South} and at ~2 km from the Sô river; finally, P_{East} is located 11.3 km southeast of P_{North} and 12.3 km northeast of P_{South}.

Each of the 4 stations consisted of an Onset HOBO U20L-01 WL logger anchored at 20-30 cm from the bottom in a perforated PVC tube of 7-cm outside diameter. Data were recorded continuously at 20-min interval between February 2018 and January 2020, with a typical accuracy of ±1 cm and a maximum error of 2 cm (https://www.onsetcomp.com/files/manual_pdfs/17153-G%20U20L%20Manual.pdf) (Wilson et al., 2016; Guragai et al., 2018).

From 30 August 2018, a Davis Vantage Pro2 weather station was installed on the roof of the Benin Institute of Fisheries and Oceanographic Research (IRHOB; Figure 1c) also recording at 20-min interval. Some of the atmospheric parameters (air temperature and humidity, precipitation rates, and winds) are used to explore the forcing mechanisms involved in high frequency WL variations (Section 3.4). However, atmospheric pressure data were overall used to correct the WL between September 2018 and January 2020. Before September 2018, WL was not corrected for barometric fluctuations, but this does not significantly alter the results and main conclusions drawn in this study. Indeed, atmospheric pressure, that varied between 1004 mbar and 1019 mbar over the available time period, exhibits two main modes of variability. First, at seasonal scale, atmospheric pressure varies by ~4 mbar, being minimum in April and maximum in August. This corresponds to a WL correction of ~4 cm which is weak compared with the seasonal WL variations of ~90 cm observed in this study (Section 3.1). Second, the stronger atmospheric pressure variability is observed at diurnal and semi-diurnal periodicities, with mean and maximum variations of ~3 and 6 mbar, respectively. This corresponds to WL variations of ~3-6 cm, of the same order than the tidal amplitudes observed in the lagoon. Thus, the tide characteristics in the lagoon (Section 3.3), are investigated using only WL data corrected from inverse barometer effects from September 2018 to December 2019.

Raw pressure data are converted to relative WLs corresponding to the height above the instrument. For each station, as no absolute vertical datum exists, the relative WLs are expressed in terms of anomalies, computed by subtracting the 20-min measurements from the seasonal mean calculated over low-water period of 2018.

No continuous in-situ ocean tide data is available. We therefore used the tidal heights computed from the last Finite Elements Solution for ocean tide (FES2014) on a 1/16° × 1/16° grid (http://www.aviso.altimetry.fr/en/data/products/auxiliary-products/global-tide-fes.html) (Carrere et al. 2016; Lyard et al. 2020). Thus, WL anomaly timeseries at P_{Ocean} (Figure 1c) was reconstructed using the 34 tidal constituents (amplitudes and phases) computed from FES2014. P_{Ocean} is located ~5.5 km to the southeast of $P_{Channel}$ (Figure 1c). FES WL at P_{Ocean} compared well with independent but irregular in-situ WL data acquired at the autonomous port of Cotonou in 2018-2019 by its hydrographic service. The correlation coefficient, mean difference, normalized root-mean-square error, and ratio of standard deviations between both datasets are 0.99, 0.02 cm, 2.7%, and 0.99, respectively.

2.3. Rainfall and river discharge data

Rainfall over the catchment was obtained from a Global Precipitation Measurement (GPM) Integrated Multi-satellitE Retrievals for GPM (IMERG) product (Huffman et al., 2014). We use the final Level 3 product developed for research applications, which is available daily on a 0.1°×0.1° longitude/latitude grid (https://gpm.nasa.gov/). Rainfall was extracted over the study period (2018-2019) and averaged in the river catchment area shown in Figure 1b. In order to filter out high frequency variability irrelevant to our study, we used monthly cumulative rainfall.

Historical estimates of the Ouémé River discharge at Bonou (~70 km upstream from the Nokoué Lagoon) and the Sô river discharge at Sô-Awa (~3 km upstream from the lagoon) are available. These daily data, available from the 1950's to the 1990's, were collected by the general Benin Directorate of water and made available by the Système d'Informations Environnementales sur les Ressources en Eau et Modélisation (SIEREM: http://www.hydrosciences.org/spip.php?article1236). A daily climatology was constructed from this multi-year dataset and the Sô and Ouémé discharges were summed to provide an estimate of the total fresh water discharge into the lagoon.

2.4. Time series analyses

The variability of the WL across temporal scales was investigated using a wavelet-based analysis (Torrence and Compo, 1998; Guo et al., 2015). The wavelet power spectrum, that estimates the spectral characteristics of the WL signal as a function of

time, is computed here using the Morlet wavelet transform. In order to compare spectral peaks across different scales, the obtained wavelet power spectra, that are slightly biased, are rectified normalizing them by the local scale (Liu et al., 2007; Veleda et al., 2012). Wavelet decomposition can also be used for signal reconstruction and filtering (Torrence and Compo, 1998). By summing over a subset of scales, we here construct WL wavelet-filtered time series in several spectral bands, from high-frequency (periods < 5h) to subtidal and low-frequency (periods > 20 days) variability.

Global power spectra obtained from wavelet analyses provide consistent estimation of the true power spectra computed from Fourier analyses (Percival, 1995). However, due to the width of the wavelet filter in Fourier space, any close peaks in Fourier spectra could be smoothed out by the wavelet analysis, particularly at small (high-frequency) wavelet scales (Hudgins et al., 1993; Torrence and Compo, 1998). Thus, in order to resolve close principal tidal constituents, their mean amplitudes and phases (e.g. Table 1) are obtained from harmonic analyses using T_TIDE package in MATLAB for each time series (Pawlowicz et al., 2002). The temporal evolution of tidal amplitudes is subsequently investigated in the diurnal (D1), semi-diurnal (D2), and quarter-diurnal (D4) spectral bands by integrating wavelet power in these specific frequency/period bands and converting them into wavelet amplitudes as in Guo et al. (2015). The D1, D2 and D4 amplitudes are computed for periods of 15-36h, 7.5-15h and 5-7.5h, respectively.

3. Results

3.1. Low-frequency variations

At the entrance of the Nokoué Lagoon at P_{South}, in the periods from February to August 2018 and from December 2018 to July 2019, the lagoon WL was low at mean WL of 0.5-0.6 m in 2018 and 0.6-0.7 m in 2019 (Figure 2a). These periods coincide with climatological periods when rivers are at baseflow and have discharges of less than ~50 m^3/s (Figure 2b). From 20 August 2018 to 30 September 2018, the mean WL increased to reach a maximum value of ~1.4 m (Figure 2a). The peak observed in 2018 coincides with the maximum climatological river discharges of ~800 m^3/s at the beginning of October. The decrease of the lagoon WL from 1.4 m to less than 0.6 m was observed between early October and early December 2018. The duration of the decrease was comparable to that of the WL rise. In contrast, the duration of increasing/decreasing WL

were strongly asymmetric in 2019. The flooding phase began in late July 2019 and took 3 months to reach the maximum of ~1.4 m on 31 October 2019. Although the beginning of the flooding phase in 2019 approximately follows the climatological river discharge, the maximum WL was observed 1 month later than the average peak of the hydrograph. In 2019, the decrease of the lagoon WL took only 1 month, and the low-WL was reached at the beginning of December, as in 2018.

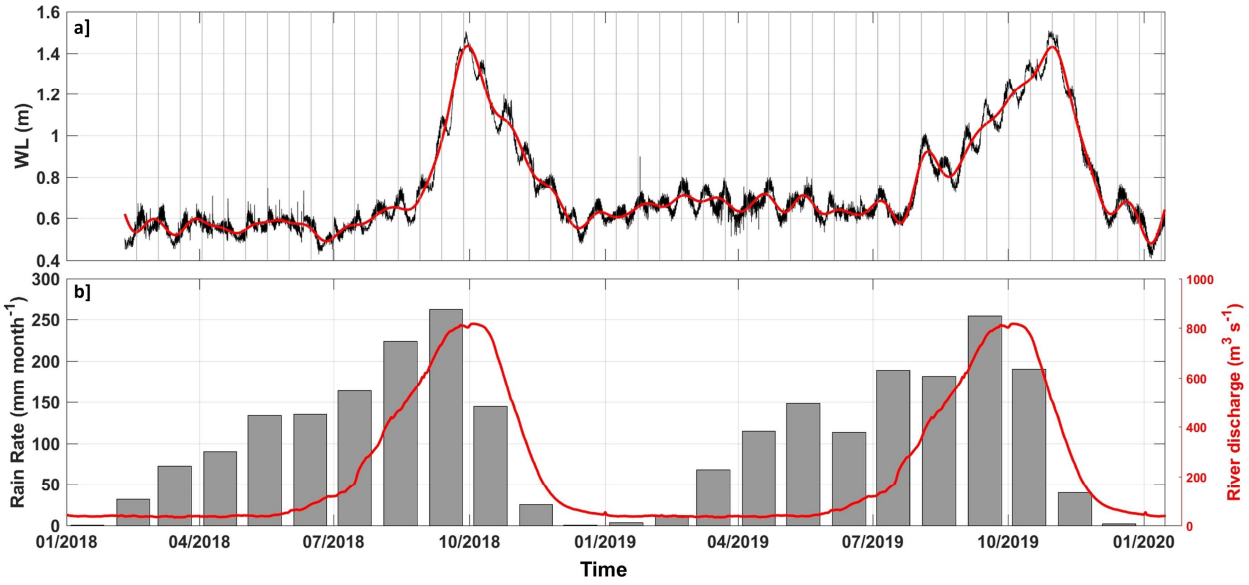

Figure 2. Water-level and hydrological variations. a] Temporal variations of the water-level (WL) at P_{South}; red line shows the low-frequency component (periods > 20 days) whereas grey vertical lines correspond to the time of oceanic spring tides. b] Monthly cumulative rainfall over the Ouémé river catchment basin (grey bars) and estimated climatological river discharge (red line).

The monthly cumulative rainfall inferred from satellite data in the Sô and Ouémé catchment basins do not show strong differences between the time periods of the rainy season of 2018 and 2019 (Figure 2b). In both 2018 and 2019, the maximum rainfalls occurred in September. However, October 2019 was 35% rainier (~190 mm) than October 2018 (~140 mm), which explains the 1-month delay observed in 2019 on the maximum WL (Figure 2a). Similarly, heavy rainfalls (~190 mm) observed in July 2019, are responsible for the earlier rise in WL in 2019, as well as for the local maximum elevation of ~0.95 m observed at the beginning of August 2019. Heavy rainfalls in July-August 2019 also contributed to spread out the flooding phase and delay the flood peak in the lagoon.

Low-frequency WL variations of the Nokoué Lagoon are related to the rainfall in the catchment basin and the river flows that discharge fresh water into the lagoon. However, superimposed on these low-frequency fluctuations, Figure 2a shows that the

unfiltered WL signal exhibits high-frequency variability patterns. The main goal of the following Sections is thus to investigate these distinct modes of variability.

3.2. WL Wavelet analysis

During the 2-year period, the 4 WL timeseries show similar patterns, not only at low-frequency (Figure 3). Superimposed on the already described low frequency WL variations, higher frequency WL variations with typical ranges of ~±20 cm that decrease from the Cotonou channel to the Nokoué Lagoon are evident (Figure 3). In order to better identify the dominant frequencies, we performed a wavelet analysis (Figures 3 and 4). WL timeseries show time-dependent variability with contributions from distinct frequency bands at certain times. Spectra can be divided into 5 main period bands, from high to low frequencies: i) high-frequency component with periods shorter than 5 hours; ii) tidal component with periods ranging between 5 hours and 1.5 days; iii) subtidal component with periods of 1.5-10 days; iv) fortnightly component with periods of 10–20 days; and v) low-frequency component with periods longer than 20 days.

The low-frequency component has been described in Section 3.1 and corresponds to large WL variations mainly due to rainfall in the catchment basins that drives the seasonal change in river discharge into the lagoon. In contrast, the subtidal component does not present significant spectral energy (Figures 3 and 4) and is thus not further investigated. Fortnightly, tidal and high-frequency components are described in more detail.

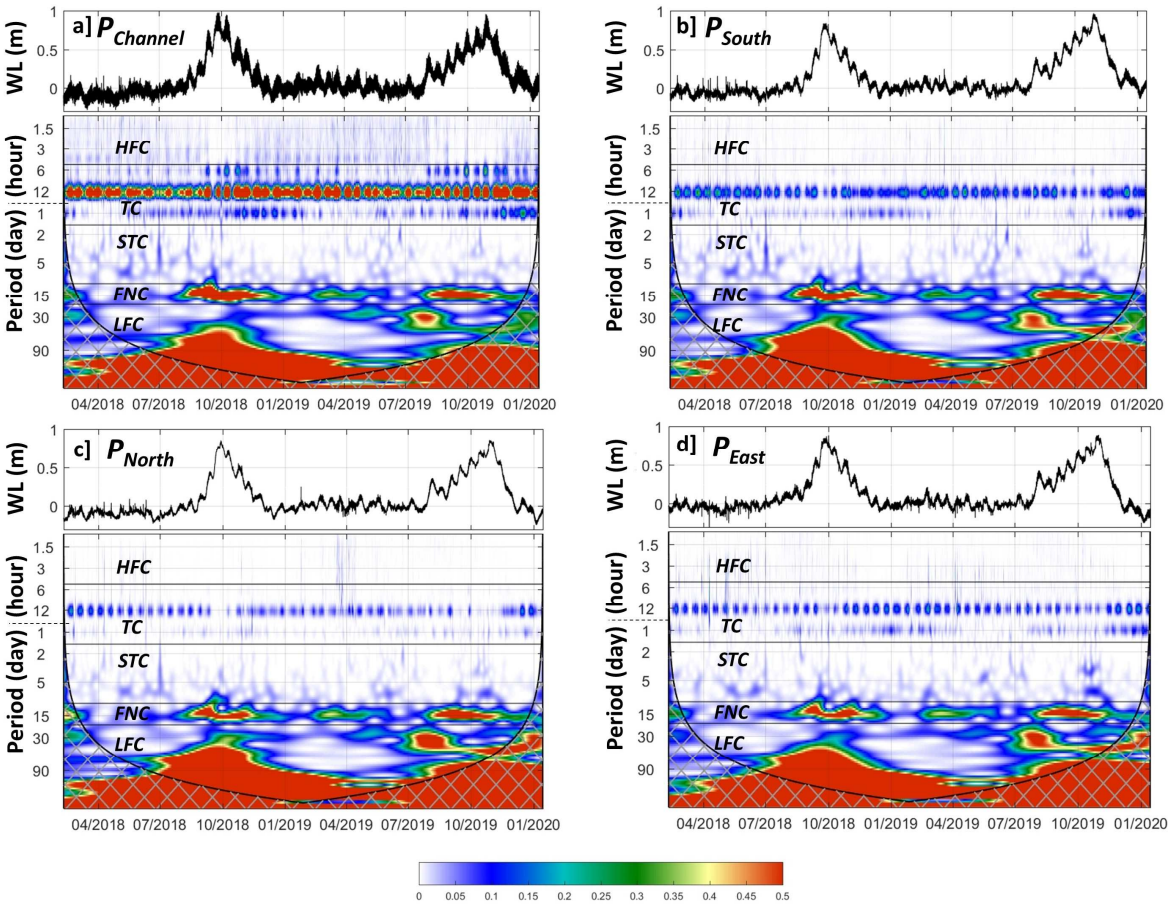

Figure 3. Water-level (WL) timeseries and corresponding rectified wavelet power spectra, at a) $P_{Channel}$, b) P_{South}, c) P_{North}, and d) P_{East}. The y axis is in day (hour, respectively) for periods higher (lower) than 1 day. The cone of influence is indicated by hatched area. Horizontal black lines on the wavelet spectra delimit 5 frequency bands: High-frequency component (HFC) (periods<5 hours); Tidal component (TC) (5-36 hours); Subtidal component (STC) (1.5-10 days); Fortnightly component (FNC) (10–20 days); Low-frequency component (LFC) (>20 days).

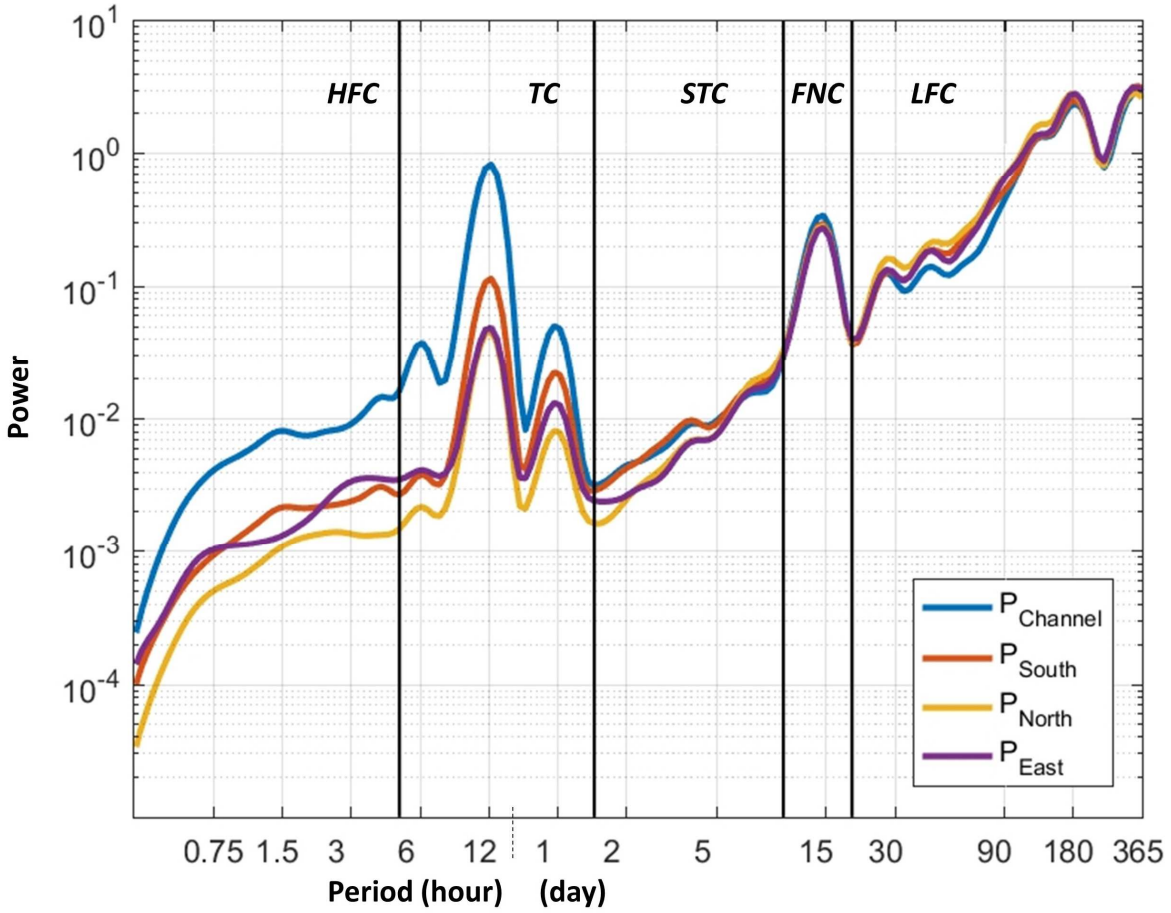

Figure 4. Global wavelet power spectra obtained by averaging over time the wavelet power spectrum at a) $P_{Channel}$, b) P_{South}, c) P_{North}, and d) P_{East}. Vertical black lines delimit the 5 frequency bands detailed in Figure 4.

3.3. Fortnightly and tidal components

a) Harmonic Analysis and main tidal constituents

Figures 3 and 4 show relatively strong spectral energy in the fortnightly (MSf) component. These oscillations of a period of ~14.8 days on the mean WL are associated with neap and spring tides. Indeed, the combination of the principal lunar (M2) and solar (S2) semidiurnal tidal constituents, characterized by very close periods (Table 1), induces a compound tide (MSf) and fortnightly variation of the oceanic semi-diurnal tide amplitude (e.g. LeBlond, 1979; Pugh, 1987). In the open-ocean, where the mean WL variations are weak compared to the tidal range, both the highest and lowest sea-levels are observed during spring tides, and the mean WL is not significantly modulated at MSf frequencies (Table 1). In contrast, in shallow lagoons or estuaries, complex non-linear interactions between oceanic semi-diurnal tides, river fluxes, bottom friction and morphology of the channel, result in MSf variations of the WL (LeBlond, 1979; Gallo and Vinzon, 2005; Guo et al., 2015). These MSf variations are observed in the Cotonou

channel and Nokoué Lagoon (Table 1), where the highest high-waters are observed during spring tides whereas the lowest low-waters are observed during neap tides (Figures 2a and 3). This is due to the fact that the tidal amplitude is generally weaker than the fortnightly variations of the mean WL (Figures 2a and 3; Table 1) induced by tidal-river interaction processes (e.g. LeBlond, 1979; Guo et al., 2015). Harmonic analyses indicate a mean MSf amplitude of ~4 cm (Table 1), which strongly increases to 10-15 cm during the wet season (not shown but see the evolution of the fortnightly component in Figure 3).

In the open-ocean off Cotonou, tides are semi-diurnal with a relatively important diurnal component (Table 1). Semi-diurnal tide constituents (A_{M2}+A_{S2}) are typically of ~70 cm amplitude whereas diurnal constituents (A_{O1}+A_{K1}) are of ~15 cm. As a result, the tidal form factor, $F = \frac{A_{O1}+A_{K1}}{A_{M2}+A_{S2}}$, which is the amplitude ratio of the diurnal to semi-diurnal tide constituents, is of 0.22, close to the mixed-tide threshold of 0.25 (Courtier, 1938). Off Cotonou, the tide is thus of semi-diurnal-dominant type, but characterized by two slightly unequal high and low tides per day. In the Cotonou channel and Nokoué Lagoon, tidal ranges are strongly dampened and the tidal form factor increases to 0.41 (Table 1). This suggests a stronger modulation of the tides at diurnal scale in the lagoon and a stronger attenuation of the semi-diurnal constituents compared to the diurnal constituents.

In shallow water, the progression of a tidal wave is modified by bottom friction and other physical processes that lead to the distortion and asymmetry of the tidal wave (Pugh et al., 1987). These non-linear effects are associated with the generation of higher harmonics such as the main M4 constituent, which is the second harmonic (or overtide) of the principal lunar tide M2, that causes disparities in the rising and falling times (e.g. Pugh et al., 1987; Gallo and Vinzon, 2005; Ray, 2007). Thus, tidal wave deformation and asymmetry are mainly due to M2-M4 interactions (e.g. Friedrichs and Aubrey, 1988; Speer and Aubrey, 1985). The general flood-dominated character of the lagoon system is highlighted by the phase difference of $2\varphi_{M2} - \varphi_{M4}$ in the range of 0-90° that leads to a longer falling tide than rising tide (Friedrichs and Aubrey, 1988; Guo et al., 2015). The magnitude of the amplitude ratio of the M4 and M2 components ($\frac{A_{M4}}{A_{M2}}$) is an indicator of the strength of the tidal asymmetry. This factor is of 0.02 at P_{Ocean} where the tide is

410 symmetric, but increases to 0.11-0.15 in the lagoon system indicating a stronger
411 asymmetry and, on average, a deformation of the tidal wave (Table 1).

412

413 *Table 1.* Average tidal properties: Tidal amplitudes (A) and phases (φ) of major diurnal (D1), semi-diurnal (D2),
414 quarter-diurnal tides (D4) and fortnightly (FNC) components' frequencies at P_{Ocean}, $P_{Channel}$, P_{South}, P_{North} and P_{East}.
415 These average tidal constituent properties were determined by harmonic analyses of 2-year WL timeseries using
416 T_TIDE (Pawlowicz et al., 2002). Periods are in hours, except for FNC frequencies where they are in days.

			P_{Ocean}		$P_{Channel}$		P_{South}		P_{North}		P_{East}	
		Period	A (cm)	φ (°)	A (cm)	φ (°)	A (cm)	φ (°)	A (cm)	φ (°)	A (cm)	φ (°)
FNC	MSf	14.77	0.0	125	4.2	60	3.9	66	4.0	70	3.9	69
	Mf	13.66	0.0	96	1.6	55	1.3	63	1.4	60	1.3	60
D1	O1	25.82	2.6	318	0.3	119	0.2	159	0.2	177	0.2	181
	P1	24.07	3.8	346	0.4	45	0.2	78	0.1	81	0.1	60
	S1	24.00	0.1	91	1.0	110	1.0	115	0.2	186	0.4	144
	K1	23.93	12.5	1	1.4	35	0.6	89	0.5	115	0.7	112
D2	N2	12.66	10.8	101	1.5	130	0.5	153	0.3	217	0.3	222
	M2	12.42	50.8	105	7.5	134	2.7	156	1.5	221	1.6	232
	S2	12.00	17.8	130	1.8	167	0.6	241	0.7	299	0.6	306
	K2	11.97	4.3	144	0.8	184	0.3	196	0.2	253	0.2	265
D4	M4	6.21	1.3	319	1.1	266	0.3	280	0.2	16	0.2	18
	MS4	6.10	0.0	104	0.7	288	0.2	299	0.1	53	0.1	48

417

418

419 **b) Tidal WL fluctuations during dry/wet seasons and spring/neap tides**

420 Figure 5 shows two-day snippets of WL fluctuations during the dry and wet
421 seasons (April and October, respectively) and for different phases of spring-neap tidal
422 cycles. During dry season spring tides (Figure 5a), the maximum tidal amplitude is of
423 ~80-90 cm in the ocean. It decreases to ~10-15 cm in the Cotonou channel and ~3-5 cm
424 in the lagoon. During this period, the average diurnal tidal amplitude (AD1) is of ~15 cm
425 in the offshore ocean and of 1-2.5 cm in the lagoon (Table 2). Similarly, the average
426 semi-diurnal tidal amplitude (AD2) varies from ~90 cm at P_{Ocean} to ~3-15 cm at the
427 other stations (Table 2). The AD1/AD2 ratio is 0.1-0.3, suggesting that the tide is mainly
428 semidiurnal without strong diurnal modulation, as seen in Figure 5a. Both the quarter-
429 diurnal amplitude (AD4) and the AD4/AD2 ratio are weak and the tide appears mostly
430 symmetric, without strong deformation.

431 During dry season neap tides (Figure 5b), the minimum tidal amplitude is of ~20
432 cm at P_{Ocean} but is strongly modulated at diurnal scale. The AD1 amplitude is ~18 cm and

AD2 decreased to ~36 cm leading to a relatively strong AD1/AD2 ratio of 0.5 (Table 2). In the lagoon, tidal amplitudes decrease to ~1-2 cm for AD1 and to 2-7 cm for AD2. These values are weaker but the associated AD1/AD2 ratios (0.3-0.7) are slightly higher to what was observed during spring tides (Figure 5a-b and Table 2). In the Cotonou channel and Nokoué Lagoon during dry season, the rising and falling tidal durations are slightly unequal and the tide is only very slightly asymmetric, as indicated by weak AD4 values of 0.1-0.2. Indeed, the ebb-tide lasts ~30-45 min longer than the flood-tide, hence the lagoon system tends to be flood-dominated (e.g. Speer et al., 1991).

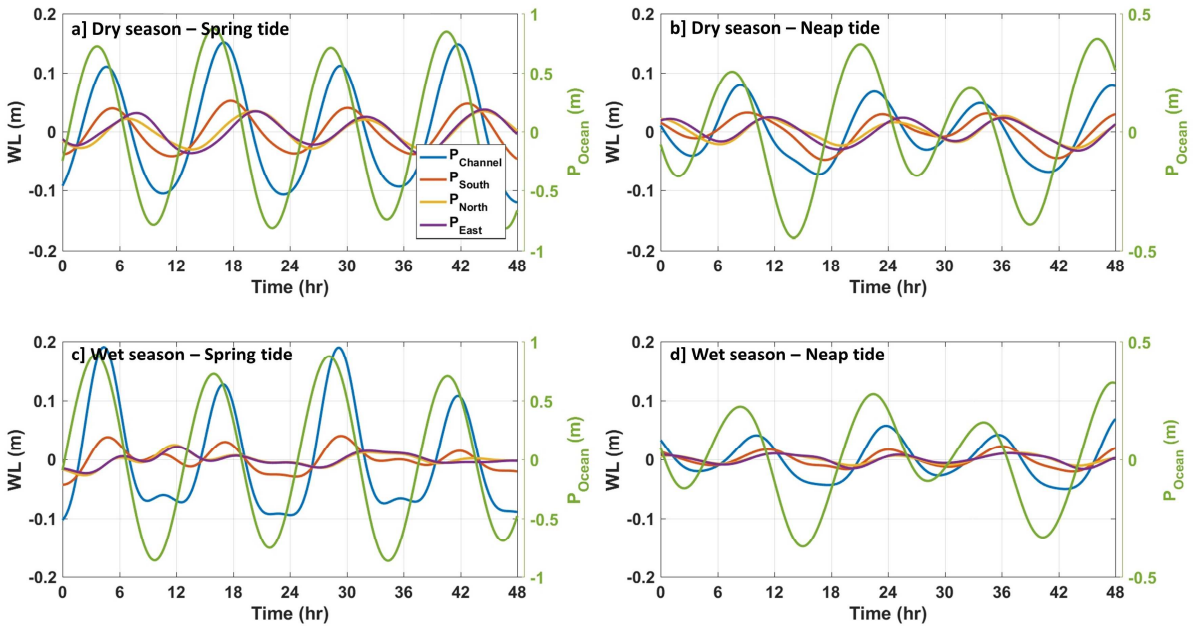

Figure 5. Examples of water-level (WL) evolution in the tidal frequency band (periods of 5-36 hr) during a] a dry season spring tide, b] a dry season neap tide, c] a wet season spring tide, d] a wet season neap tide. WL at $P_{Channel}$, P_{South}, P_{North}, and P_{East} correspond to left axes whereas WL at P_{Ocean} correspond to right axes.

During the wet season, the tide characteristics in the open ocean are similar to the dry season, with AD1 of ~15 cm and AD2 varying from ~95 cm for spring tides to ~30 cm for neap tides (Figure 5c-d and Table 2). In contrast, tide characteristics are significantly modified in the channel and the lagoon, and more particularly during wet season spring tides (Figure 5c). AD2 decreases during wet season and AD1 tends to increase (see also wavelet power spectra in Figure 3). The tidal form factor AD1/AD2 increases from ~0.1-0.7 during the dry season, to 0.5-2.2 during the wet season (Table 2), as a result of a stronger modulation of the tides at diurnal scale during high water periods. During spring tides (Figure 5c), the flood duration is 4-5 h, whereas the ebb-

tide lasts 7-8 h. Notably the wave shape of the tides tends to be positively skewed with a slack-tide asymmetry, in particular at $P_{Channel}$ (blue line in Figure 5c). This slack-tide asymmetry is due to a phase difference between M2 and M4 ($2\varphi_{M2} - \varphi_{M4}$) that is, on average, close to 0° (Table 1) (e.g. Guo et al., 2019).

Finally, high and low tides are systematically observed 1 hour later at $P_{Channel}$ than at P_{Ocean} (Figure 5). In contrast, the high or low tide phase shift between P_{South} and P_{North} or P_{East}, varies from 1h-3h during dry season (Figure 5a,b) and is strongly uncertain during wet season when the tide is much more asymmetric and deformed (Figure 5c,d). Note also that winds can impact WL in shallow lagoons, in particular by pushing and piling up water in the downwind direction (e.g. Stieglitz et al., 2013; Colvin et al., 2018). However, data from the weather station reveals that the dominant southwest wind is weak and varies from 2.2. m s^{-1} in December to 4.5 m s^{-1} in August. Similarly, at diurnal scale, the wind only varies by 2 m s^{-1}, being minimum at 6-7 am and maximum at 3-4 pm. Considering a steady state balance between the wind-stress and the barotropic pressure gradient generated by the slope of the free surface, these typical winds would result on wind setups of ~1-3 cm in the northeastward direction (see equations in e.g. Colvin et al., 2018). This weak signal could not be evidenced in the WL dataset, and no significant WL slope was observed between P_{North}/P_{East} and P_{South}, neither at seasonal nor diurnal scales. However, as described in the following Section, high-frequency fluctuations of the wind field generate high-frequency variations of the WL slope in Nokoué Lagoon.

Table 2. Average tidal amplitudes of diurnal (AD1), semi-diurnal (AD2), and quarter-diurnal tides (AD4) at P_{Ocean}, $P_{Channel}$, P_{South}, P_{North} and P_{East} and for 4 selected 48-hour periods. Amplitude ratios (AD1/AD2 and AD2/AD4) are also indicated. These average tidal constituent properties were determined by integrating wavelet powers in specific frequency/period bands (15-36h for D1, 7.5-15h for D2, and 5-7.5h for D4). Amplitudes are in cm.

	P_{Ocean}	$P_{Channel}$	P_{South}	P_{North}	P_{East}
			Dry Season – Spring Tide		
AD1	13.3	2.6	0.9	1.0	1.0
AD2	94.2	14.2	5.1	3.4	3.5
AD4	3.8	2.0	0.6	0.3	0.4
AD1/AD2	0.14	0.18	0.17	0.30	0.29
AD4/AD2	0.04	0.14	0.12	0.10	0.11
			Dry Season – Neap Tide		
AD1	17.6	3.1	2.2	0.6	1.1
AD2	36.0	6.7	3.2	2.4	2.7

AD4	1.9	1.2	0.5	0.4	0.3
AD1/AD2	0.49	0.47	0.70	0.26	0.42
AD4/AD2	0.05	0.18	0.15	0.18	0.13
		Wet Season – Spring Tide			
AD1	14.9	3.3	1.8	1.5	1.5
AD2	95.3	14.0	2.7	0.7	0.7
AD4	3.8	5.7	1.5	0.8	0.7
AD1/AD2	0.16	0.24	0.68	2.06	2.24
AD4/AD2	0.04	0.41	0.57	1.02	1.01
		Wet Season – Neap Tide			
AD1	16.6	2.1	0.6	0.5	0.6
AD2	28.0	5.1	1.9	1.0	1.1
AD4	1.7	1.0	0.5	0.2	0.3
AD1/AD2	0.59	0.41	0.34	0.54	0.53
AD4/AD2	0.06	0.21	0.24	0.21	0.28

3.4. High-frequency component (periods < 5 hours)

Relatively strong HF variability was observed between February and June 2018, October-November 2018, and February to June 2019 (Figure 6a). For example, during a 2-week period in 2018, 4 individual HF events were observed (Figure 6b). These high-frequency fluctuations can be either in phase or in opposition between the different stations. Typical oscillations of ±5-10 cm are observed.

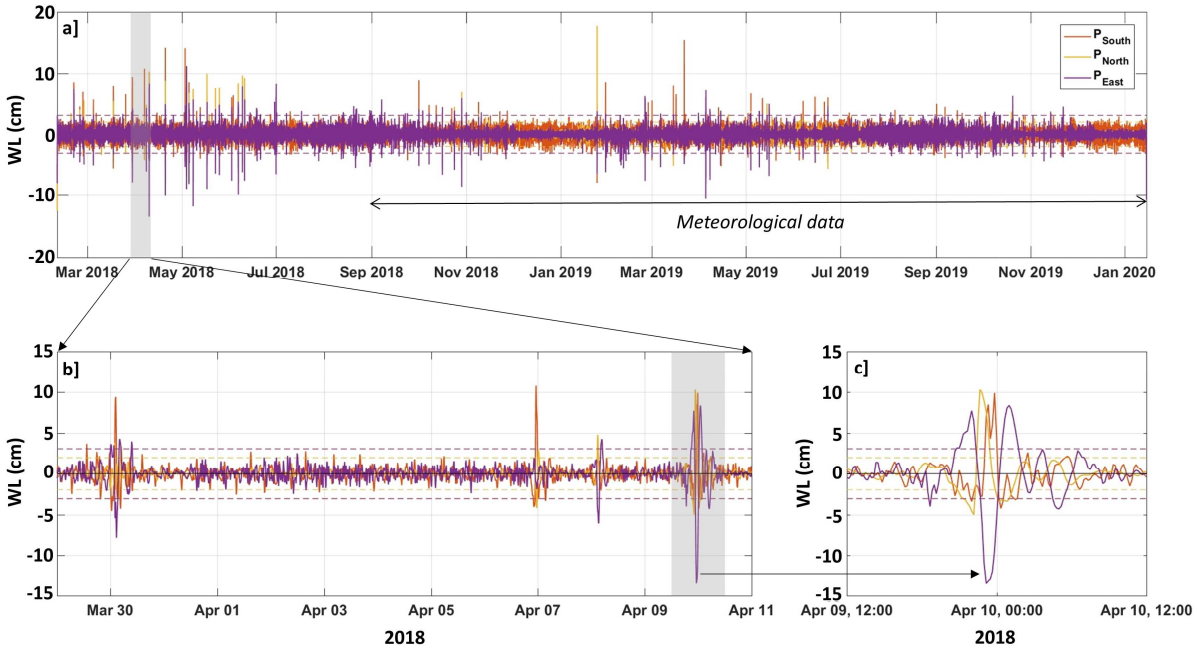

Figure 6. High-frequency component (HFC) of the water level evolution in the Nokoué Lagoon. a] HFC (periods < 5 hours) for the 2-year study period (2018-2019), showing strong HF events. b] HFC for a 12-day period. c] A particular HF event observed in April 10, 2018. In these figures, horizontal dashed lines correspond to ±4 standard deviations around the mean and are used to automatically detect HF events associated with seiches.

As an example, Figure 6c shows the HF WL variations for the particular event that occurred during the night 09-10 April 2018. Between 08:00 and 10:00 pm, the WL increased by ~7-8 cm in the eastern part of the lagoon (P_{East}) at a simultaneous decrease of 4-5 cm at P_{South} and P_{North}. Thus, this rapid evolution generated a WL difference of 12-13 cm between the East and the central line of the lagoon joining P_{South} and P_{North}. After 10:00 pm, the WL rapidly decreased (increased, respectively) at P_{East} (P_{South} and P_{North}) to reach a maximum negative (positive) anomaly of -13.5 cm (+10 cm) between 11:00 pm and midnight (Figure 6c). This led to a maximum WL difference of ~23 cm between the eastern and central parts of the lagoon. Subsequently, the WL began to oscillate around its equilibrium value with amplitudes of a few cm. These oscillations,

characterized by a period of ~2h45min, were rapidly dissipated on 10 April after 08:00 am. This ~12-hour duration event, characterized by regular WL free standing-wave oscillations that are progressively dampened, is typical of a seiche event as frequently observed in other lakes, lagoons or coastal embayments (e.g. Chapman and Giese, 2001). For this particular event, the observed standing-wave oscillation period of 2h45min is in close agreement with the Merian's theoretical period of a seiche oscillation in a rectangular flat-bottom basin (Chapman and Giese, 2001): considering the larger dimension of the Lagoon (L = 20 km) and a mean depth (H) of 1.3 m, the Merian's theoretical period value ($T = \frac{2L}{\sqrt{gH}}$) is of ~3h.

In order to better characterize such HF events, and to provide a more robust description of their main characteristics, a composite analysis was performed. First, individual HF events were filtered as any event associated with a strong WL increase at a given lagoon station (P_{South}, P_{North}, and P_{East}) and a simultaneous strong WL decrease in another gauged station. In order to ensure a high confidence level and exclude any potential false detection, a strong increase/decrease is defined as higher than +/- 4 standard deviations from the mean (Figure 6). Peaks with such high variations occur less than 0.1% of the time. A total of 44 HF events, significantly impacting at least 2 WL stations, were detected. Interestingly, more than 75% (34 on 44) of these events were associated with a strong WL minimum in the eastern part of the lagoon at P_{East}, as also observed in Figure 6c. In terms of seasonality, about 85% of the 44 HF events took place during the dry season between February and June and none of them between August and September.

Second, since the lagoon is elongated in East-West direction and seiche phenomena are expected to more likely develop along the elongated direction, we selected only HF events characterized by a significant WL minimum at P_{East}. Furthermore, after visual inspections, we retained 32 events characterized by similar evolutions in meteorological parameters. Figure 7a displays the composite analysis of the WL evolution for these 32 events, obtained by centering each event at the time the WL minimum at P_{East} was observed (t=0h in Figure 7). On average, about 3 hours before the start of the seiche, the WL gently rises by 2 cm to the East and decreases by ~1 cm at P_{South} and P_{North}. Note that the seiche is triggered at time t=-1.5h, when the WL starts to decrease (increase respectively) at P_{East} (P_{South} and P_{North}). The WL anomaly reaches its minimum value (-5 cm) at P_{East} at t=0h, while maximum WL anomalies (~2 cm) are

observed at P_{North} and P_{South} at t=-0.5h and t=+0.5h respectively. Then, as observed for the individual event shown in Figure 6, the WL oscillates with inverse anomalies between P_{East} and P_{North}/P_{South} (Figure 7a), with an oscillation period of ~3h-3h30. The dissipation is much faster that the single event analyzed in Figure 6, due to the averaging of 32 events that can be characterized by slightly different periods and amplitudes.

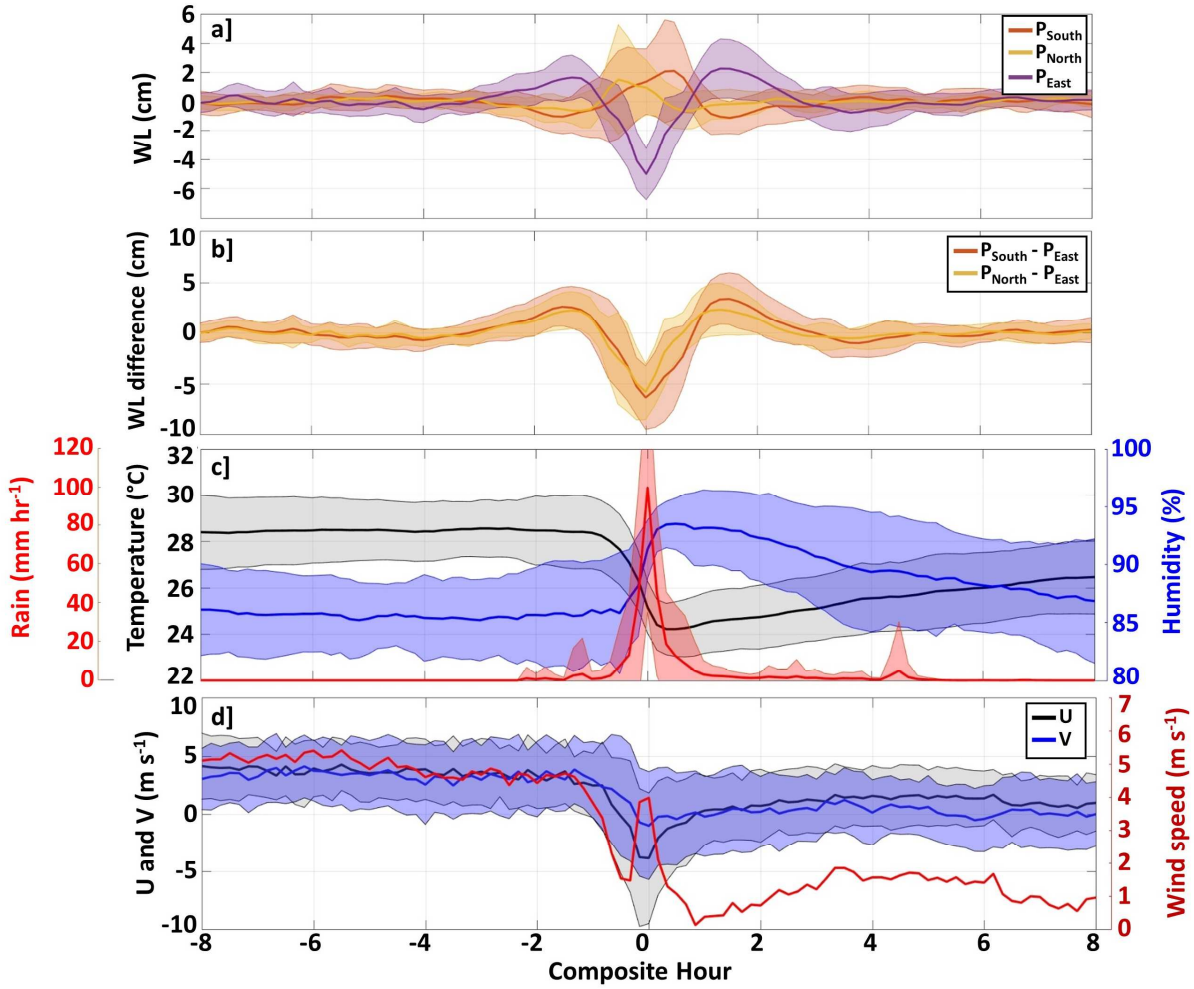

Figure 7. Composite analysis of seiche events and associated atmospheric parameters. a] Averages of water-level (WL) evolution at P_{South}, P_{North} and P_{East} for the 32 HF events associated with a maximum negative WL anomaly at P_{East} at t = 0. b] Mean WL differences between P_{South} and P_{East} and between P_{North} and P_{East}. c] Mean air-temperature, air-humidity and rain. d] Mean wind velocity components (left axis) and wind speed (right axis). Color shading correspond to ±1 standard deviation around the means. In order not to overload the figure, standard deviations are not shown for wind speed in c].

Finally, in order to better understand the forcing mechanisms involved in the seiche generation, a composite analysis of some key meteorological parameters was performed (Figure 7c-d). Leading up to the seiche triggering, atmospheric conditions are relatively stable with on average an air temperature of ~28.5°C, a humidity of ~85%,

and no rain (Figure 7c). The wind is also regular, blowing towards the Northeast (zonal and meridional components are equal and positive) with a mean speed of 4-5 m s^{-1} (Figure 7d). This wind regime tends to accumulate water in the Northeast/East of the lagoon as observed in Figure 7a. At the start of the seiche (t=-1.5h) the wind suddenly decreases and progressively reverses (Figure 7d). At t=0, when the WL is minimum at P_{East}, the wind blows towards the West-Southwest with a mean speed of ~4 m s^{-1} (Figure 7d). This strong and rapid wind inversion is thus the main forcing mechanism of the seiche, causing the displacement of the water from the East to the West and initiating the WL oscillations. After this maximum wind inversion, the wind progressively blows again towards the Northeast but with a very weak intensity (< 2 m s^{-1}). Interestingly, during the seiche event the air temperature suddenly drops by 4-5°C, the humidity increases to reach an average value of 93% and very strong rain events are observed (Figure 7c). These showers of up ~100 mm/h rainfall have a duration of 30-60 min. These patterns are likely related to the passage of fast-moving squall-lines, characterized by strong pressure jumps and downdraft winds, with short but intense rainfalls (e.g. Omotosho, 1984; 1985; Schrage and Fink, 2007). Interestingly, the seasonal variation of the number of squall-lines in West African coastal regions, shows a bi-modal distribution with a strong maximum in March-June and almost no squall-line in July-September (Omotosho, 1984; 1985). Both the number of squall-lines and the number of seiche events show similar seasonal variations (85% of the seiche events were observed in February and June and none in August-September), which strongly suggests that the passage of these atmospheric disturbances (squall-lines) are likely responsible of the observed seiche phenomena.

4. Discussion

4.1. Subtidal WL variations

This study complemented previous limited studies (Le Barbé et al., 1983; Djihouessi and Aina, 2018), highlighting the main roles of river runoffs, tides and winds in the WL variations of Nokoué Lagoon. Observed low-frequency subtidal WL variations of ~0.8-0.9 m are the result of the importance of continental water inflow and the lagoon's evacuation capacities, which depend on the ocean level. At regional scale, the WL has only been measured in the Ebrié Lagoon (Ivory Coast) for 1-year in 1952. This lagoon also showed an

increase of 50 cm during watershed flooding in October-November (Varlet, 1978; Durand and Guiral, 1994). In Nokoué Lagoon, our results suggested a 1-month delay between maximum rainfall in the catchment basin and the maximum WL in the lagoon, which is encouraging to elaborate an operational seasonal flood forecasting system in the lagoon from rainfall observations.

Our study also suggests that such forecasting system has to take into account tide forcing. The interaction of M2 and S2 tidal constituents through non-linear bottom friction and river interaction resulted in a pronounced fortnightly-period oscillation of lagoon WL, as expected from one-dimensional simplified models (e.g. Hill, 1994; MacMahan et al., 2014).

4.2. Tidal WL variations

Tides are strongly attenuated, with a main semidiurnal (M2+S2) tidal amplitude decreasing from 30-90 cm in the ocean to ~1-3 cm in the Nokoué Lagoon (see Table 2 and also Zandagba et al., 2016). The tidal signal is thus altered by the frictional channel that acts as a dynamic low-pass filter (Kjerfve and Magill, 1989) and the Nokoué Lagoon can be classified as a choked coastal lagoon (Kjerfve, 1986) with a choking coefficient varying with the season and ocean tide amplitude (Table 3).

Based on Stigebrandt (1980), many studies have explained choking conditions using a simple one-dimensional model (e.g. Rydberg and Wickbom, 1996), where the response of the WL within the lagoon (η_{lagoon}) to the ocean sea-level forcing (η_{ocean} and M2 tide) and a variable freshwater supply (Q_{river}) is given by:

$$\frac{d\eta_{lagoon}}{dt} = P\frac{\eta_{ocean}-\eta_{lagoon}}{\sqrt{|\eta_{ocean}-\eta_{lagoon}|}} + S \qquad (1)$$

where the parameters characterizing the choking conditions are (Stigebrandt, 1980):

$$P = \frac{hl}{A\sqrt{1+\lambda}}\sqrt{\frac{2gT^2}{a_{ocean}}} \qquad \lambda = 2\kappa\frac{L}{h} \qquad \text{and} \qquad S = \frac{Q_{river}T}{Aa_{ocean}}$$

with g = 9.81 m/s^2 is the gravitational acceleration; T = 12.42 hours and a_{ocean} = 0.5 m, are the M2 tidal period and amplitude in the ocean, respectively; κ ~ 0.003 is a friction coefficient used in quadratic friction laws (e.g. Robinson et al., 1983; Stigebrandt and Molvær, 1988; Sternberg, 1968; Rydberg and Wickbom, 1996); A = 170 km^2 is the lagoon area, L = 4000 m the length of the Cotonou channel, l = 280 m its breadth, and h = 3 m its depth. The river

discharge, Q_{river}, is poorly known but estimated climatologies show it varies from ~50 m^3 s^{-1} in low-water season to ~800 m^3 s^{-1} during flood period (Figure 2).

Table 3. Tidal choking coefficients (in bold) obtained from average semidiurnal tidal amplitudes observed in the ocean (a_{ocean}) and Nokoué Lagoon (a_{lagoon}), and from theoretical results from Equation 1 (Stigebrandt, 1980) for different hydrological periods (dry and wet seasons) and tidal characteristics (spring and neap tides). a_{lagoon} was obtained from Table 2, averaging semidiurnal tidal amplitudes (AD2) at the 3 stations located in Nokoué Lagoon (P_{South}, P_{North}, P_{East}).

	Observations			*Theoretical (Stigebrandt, 1980)*		
	$a_{ocean}\ (cm)$	$a_{lagoon}\ (cm)$	$C_c = \frac{a_{lagoon}}{a_{ocean}}$	C_C	P	S
			Dry Season (Q_{river} = 50 m^3 s^{-1})			
Spring Tide	94.2	4.0	**0.04**	**0.06**	0.34	0.01
Neap Tide	36.0	2.8	**0.08**	**0.09**	0.54	0.04
			Wet Season (Q_{river} = 800 m^3 s^{-1})			
Spring Tide	95.3	1.4	**0.01**	**0.02**	0.33	0.22
Neap Tide	28.0	1.3	**0.05**	**0.06**	0.62	0.75

In this model, tidal choking depends at first order upon the geometrical characteristics of the lagoon and channel including friction effects (e.g. Stigebrandt, 1980; Hill, 1994; MacMahan et al., 2014). River outflows plays an additional role in modifying both the mean lagoon WL and the tidal amplitude and phase (Stigebrandt, 1980). Given the lagoon and river discharge characteristics, we obtain λ ~ 8 indicating a strong control of tidal choking by bottom friction. *P* varies from 0.3 for spring semidiurnal tides to 0.6 for neap tides (Table 3). Interestingly, because of extreme hydrological variability, *S* varies from 0.01 in dry season to 0.8 in wet season (Table 3), implying a strong influence of river discharge for the choking process. Following Stigebrandt (1980; see his Table 1), the predicted choking coefficient varies from 0.02 to 0.09 (Table 3). These results only slightly differ from our estimates (Table 3), in particular because river inflow is poorly known. This good agreement shows that this simple model is able to explain the observed choking conditions and its strong seasonal and fortnightly variability.

Also, for the considered river outflows (50 and 800 m^3 s^{-1}) the Stigebrandt's (1980) theory predicts a similar tidal asymmetry in the lagoon, with an ebb duration ~35 min longer than the flood. This is in agreement with what we observed during dry season (30-45 min), but the observed ebb-flood asymmetry was stronger during flood period. The expected phase delay between high water in the ocean and in the lagoon is predicted to be of 1.5-3 hours (longer phase shifts for stronger river outflows), in agreement with the values observed in Section 3.3b. Furthermore, Stigebrandt (1980) suggested from his theory that the mean WL in

653 the lagoon would increase by 5 cm in low-water period and ~80 cm during flood season,
654 which is very close to our observations (Figure 2). These comparisons between observed and
655 predicted values from the Stigebrandt's (1980) theory at different timescales are very
656 promising for using this simplified one-dimensional models to predict WL in Nokoué Lagoon
657 from river discharge data and tidal constituents. Implementing a forecasting system was
658 beyond the scope of the present study, but this problem and approach will deserve future
659 studies.
660
661 ### 4.3. High-frequency WL variations
662 Finally, as shown in Section 3.4, the HF WL acquisition rates allowed us to highlight
663 the occurrence of seiches in Nokoué Lagoon and to provide their main characteristics. These
664 HF events, forced by the passage of fast-moving squall lines, are characterized by typical WL
665 oscillations of ±5-10 cm. Seiches are commonly observed in large lakes or lagoon in the
666 World (e.g. Chapman and Giese, 2001). However, due to the lack of continuous WL
667 monitoring, these HF events have been only marginally documented in some lakes of Central
668 and East Africa (e.g. Beauchamp, 1939; 1953; Jollyman, 1955; Fish, 1957; Ward, 1959). In
669 West-Africa, only Varlet (1978) mentioned the occasional existence of damped oscillations in
670 the Ebrié Lagoon whose amplitude could reach 10 cm and whose period was about thirty
671 minutes. He also noted that in 1952, a tornado produced a momentary rise of 5-15 cm in the
672 Ebrié lagoon. Our study, based on a robust statistical analysis, provides an unprecedented
673 description of the seiche phenomenon in an African coastal lagoon. These results provide
674 useful metrics to validate barotropic shallow-water models, that in turn could be used to better
675 understand seiche dynamics in Nokoué Lagoon. They also suggest that, to be exhaustive,
676 flood forecasting system should incorporate or parameterize seiche oscillations in Nokoué
677 Lagoon.
678
679 # 5. Conclusion
680 ### 5.1. Summary of the results
681 In this study we analyzed new WL data of a poorly observed West African lagoon.
682 High frequency (20 min) and long term (2 years) observation of the Nokoué lagoon WL
683 were analyzed and revealed a strong variability in 4 main frequency bands.
684 First, the known seasonal variability, associated with the West-African Monsoon,
685 causes the WL in the lagoon to increase by ~0.9 m between low and high water periods.

We observed interannual variability, and related them to variations of rainfall over the watershed and associated river discharge, but the lack of available contemporary hydrological and meteorological data prevents any further diagnostics.

Second, for the first time in this lagoon, we revealed strong fortnightly frequency variations of the mean WL in the lagoon, with the highest high-waters observed during spring tides and the lowest low-waters during neap tides. Amplitudes of the fortnightly variations are much higher (10-15 cm) during the wet season. This process has to be associated to nonlinear interactions of oceanic tidal constituents (Hill, 1994) but the details of the mechanism has to be investigated using a model.

Third we showed that, at (semi)diurnal scale, there is a strong attenuation of the tidal range within the Cotonou channel and the Nokoué lagoon is flood-dominated. On average, semi-diurnal (diurnal, respectively) tidal amplitudes decreases from ~70 cm (15 cm) in the ocean to ~2-3 cm (<2 cm) within the lagoon. We showed that the Stiegebrandt (1980) tidal choking model explains this phenomenon: the long Cotonou channel connecting the Lagoon to the ocean, acts as a natural low-pass filter that reduces tidal effect in the lagoon but increase the fortnightly component, and more particularly during wet season when river discharge is high.

Fourth, we observed higher frequency WL variability, characterized by periods shorter than 5 h. Most of these energetic events are observed during the dry season, and are associated with typical WL variations of 5-10 cm. We showed that these HF patterns correspond to wind-forced seiches associated with the passage of fast-moving squall-lines. The perturbation of the persistent southwest winds by the passage of these atmospheric disturbances leads to the development of seiches with a period of ~3 h. During these events, that are rapidly dissipated, heavy rainfalls are observed and the air temperature drops on average by 5°C.

5.2. Perspectives: towards the development of a flood forecasting model

Floods are one of the most devastating natural hazards in West Africa, increasing in frequency, magnitude and impact in recent decades (Aerts et al., 2014; Di Baldassarre et al., 2010; Ekeu-Wei, 2018). Various west-African political and economic capitals are concerned by flooding, in particular due to their proximity to coastal lagoons fed by important watersheds (e.g. Lagos in Nigeria, Cotonou in Benin, Lomé in Togo, Abidjan in Ivory Coast, etc.). Local governments therefore require information to implement appropriate flood

management measures. However, the acquisition and maintenance of environmental and climate observation networks in these developing regions is very challenging, despite their vulnerability to climate variability and change (Ampadu et al., 2013; Eku-Wei, 2018 ; Dinku, 2019 ; Brocca et al., 2020). As such, WL timeseries in West-African lagoons are rare or non-existent. The observations and diagnostics presented in this study contribute to a better understanding of the dynamics of the Nokoué Lagoon, and form a scientific base to inform an improved management of flood risks of the adjacent low-lying coastal cities. Indeed, our study demonstrates that a flood early warning system must not only consider the hydrological regime of the catchment (Sô and Ouémé rivers), but also the propagation and non-linear interactions of the ocean tide that produces significant WL fluctuations of Nokoué Lagoon, in particular at fortnightly periods during flood season. In a second step, this flood warning system should also include seiches that give rise to high frequency WL oscillations which can cause additional surges.

Acknowledgments.

Field campaigns and instrumentation were supported by IRD, IRHOB and ANR @RAction chair medLOC (ANR-14-ACHN-0007-01–T.Stieglitz). V. OKPEITCHA was funded by OmiDelta project of the Embassy of the Netherlands in Benin, through a scholarship grant of the National Institute of Water (INE). This work is a contribution to the « JEAI SAFUME » project funded by IRD. Special thanks to the members and crew participating to the deployment and recovery of the sensors, and in particular to Joseph AZANKPO.

References.

Adandedjan, D., Makponse, E., Hinvi, L.C., Lalèyè. P., 2017. Données préliminaires sur la diversité du zooplancton du lac Nokoué (Sud-Bénin). Journal of Applied Biosciences 115, 11476–11489.

Adite, A., and Winemiller, K.O., 1997. Trophic ecology and ecomorphology of fish assemblages in coastal lakes of Benin, West Africa. Écoscience 4 (1), 6-23.

Adite, A., ImorouToko,I., Gbankoto, A., 2013. Fish Assemblages in the Degraded Mangrove Ecosystems of the Coastal Zone, Benin, West Africa: Implications for Ecosystem Restoration and Resources Conservation. Journal of Environmental Protection 4 (12), 1461-1475.

Adjahouinou, D.C., Liady, N.D., Fiogbe, E.D., 2012. Diversité phytoplanctonique et niveau de pollution des eaux du collecteur de Dantokpa (Cotonou-Bénin), Int. J. Biol. Chem. Sci. 6 (5), 1938-1949.

Adjahouinou, D.C., Yehouenou, B., Fiogbe, E.D., Liady, M.N.D., 2014. Caractérisation bactériologique des eaux résiduaires brutes de la ville de Cotonou (Benin). Journal of Applied Biosciences 78, 6705 – 6713.

Aerts, J. C., Botzen, W. W., Emanuel, K., Lin, N., De Moel, H., Michel-Kerjan, E. O., 2014. Evaluating flood resilience strategies for coastal megacities. Science, 344(6183), 473-475.

Ahouangan, M.B.D., Djaby, B., Ozer, P., Hountondji, Y.C., Thiry, A., De Longueville, F., 2014. Adaptation et résilience des populations rurales face aux catastrophes naturelles en Afrique subsaharienne. Cas des inondations de 2010 dans la commune de Zagnanado, Bénin. In: Ballouche, A. & Taïbi, N. A. (Eds.), Eau, milieux et aménagement. Une recherche au service des territoires. Presses de l'Université d'Angers, Angers, France, pp. 265-278.

Ahokpossi, Y., 2018. Analysis of the rainfall variability and change in the Republic of Benin (West Africa), Hydrological Sciences Journal 63 (15-16), 2097-2123.

Aina, M. P., Degila, H., Chikou, A., Adjahatode, F., Matejka, G., 2012a. Risk of intoxication by heavy metals (Pb, Cd, Cu, Hg) connected to the consumption of some halieutic species in lake Nokoué: case of the Penaus schrimps and the Sarotherodon Melanotheron. British Journal of Science 5 (1), 104-118.

773 Aina, M.P., Djihouessi, B., Vissin E.W., Kpondjo, N.M., Gbèdo, V., Sohounhloué K.C.D.,
774 2012b. Characterization of the domestic wastewaters and dimensionality of a pilot
775 treatment station by lagooning at Abomey Calavi city- Benin. J. Engineering Sci. 1 (1),
776 45-50.
777 Allersma, E., Tilmans, W.M.K., 1993. Coastal Conditions in West Africa: A Review. Ocean
778 and Coastal Management 19, 199-240.
779 Ampadu, B., Chappell, N. A., Kasei, R. A., 2013. Rainfall-Riverflow modelling approaches:
780 making a choice of data-based mechanistic modelling approach for data limited
781 catchments: A review. Canadian Journal of Pure and Applied Sciences, 7(3), 2571-
782 2580.
783 Aubrey, D.G., Speer, P.E., 1985. A study of non-linear tidal propagation in shallow
784 inlet/estuarine systems Part I: Observations. Estuarine Coastal Shelf Science 21, 185–
785 205.
786 Beauchamp, R.S.A., 1939. Hydrology of Lake Tanganyika. Int. Rev. ges. Hydrobiol. 39,
787 316-353.
788 Beauchamp, R.S.A., 1953. Hydrological data from Lake Nyasa. J. Ecol. 41, 226-239.
789 Biao, E. I., 2017. Assessing the impacts of climate change on river discharge dynamics in
790 Ouémé river basin (Benin, West Africa). Hydrology 4 (47).
791 Brocca, L., Massari, C., Pellarin, T., Filippucci, P., Ciabatta, L., Camici, S., Kerr, Y.H.,
792 Fernández-Prieto, D., 2020. River flow prediction in data scarce regions: soil moisture
793 integrated satellite rainfall products outperform rain gauge observations in West
794 Africa. Scientific Reports, 10(1), 1-14.
795 Brookes, J., Povilanskas, R., Khokhlov, V., 2018. Assessing, quantifying and valuing the
796 ecosystem services of coastal lagoons. Journal for Nature Conservation 44, 50-65.
797 Carrere L., Lyard, F., Cancet, M., Guillot, A., Picot, N., 2016. FES 2014, a new tidal model -
798 Validation results and perspectives for improvements, presentation to ESA Living
799 Planet Conference, Prague 2016.
800 Chapman, D. C., Giese, G.S., 2001. Waves: Seiches, in Encyclopedia of Ocean Sciences 5,
801 edited by J. H. Steele, K. K. Turekian, and S. A. Thorpe, pp. 2724–2731, Academic,
802 London.
803 Choplin, A., 2019. Produire la ville en Afrique de l'Ouest : le corridor urbain de Accra à
804 Lagos. L'Information géographique 83 (2), 85–103.

Colleuil B. (1987). Le complexe lagunaire du Lac Nokoué et de la lagune de Porto-Novo (Bénin). In : Burgis M.J. (ed.), Symoens J.J. (ed.), Gac Jean-Yves (coord.). African wetlands and shallow water, Paris : ORSTOM, (211), 188-196.

Colvin, J., Lazarus, S., Splitt, M., Weaver, R., and Taeb, P. 2018. Wind driven setup in east central Florida's Indian River Lagoon: Forcings and parameterizations. Estuarine, Coastal and Shelf Science, 213, 40-48.

Courtier, A., 1938. Marées. Service Hydrographique de la Marine, Paris, available at : https://journals.lib.unb.ca/index.php/ihr/article/download/27428/1882520184 (last access: 24 December 2020).

Di Baldassarre, G., Montanari, A., Lins, H., Koutsoyiannis, D., Brandimarte, L., Blöschl, G., 2010. Flood fatalities in Africa: from diagnosis to mitigation. Geophysical Research Letters, 37(22).

Dinku, T., 2019. Challenges with availability and quality of climate data in Africa. In Extreme hydrology and climate variability. Elsevier. 71-80.

Djihouessi, M.B., Aina, M.P., Kpanou, B.V., Kpondjo, N., 2017. Measuring the Total Economic Value of Traditional Sand Dredging in the Coastal Lagoon Complex of Grand-Nokoue (Benin). Journal of Environmental Protection 8, 1605-1621.

Djihouessi, M.B., Aina, M.P., 2018. A review of hydrodynamics and water quality of Lake Nokoué: current state of knowledge and prospects for further research. Reg. Stud. Mar. Sci. 18, 57–67.

Djihouessi, M.B., Djihouessi, M.B., Aina, M.P., 2019. A review of habitat and biodiversity research in Lake Nokoué, Benin Republic: Current state of knowledge and prospects for further research. Ecohydrology and Hydrobiology 181, 1-15.

Duck, R. W., da Silva, J. F., 2012. Coastal lagoons and their evolution: a hydromorphological perspective. Estuarine, Coastal and Shelf Science 110, 2-14.

Durand, J. R., Guiral, D., 1994. Hydroclimat et hydrochimie. In : Environnement et ressources aquatiques de Côtes d'Ivoire. Tome 2 : les milieux lagunaires, Durand J. R., Dufour P., Guiral D. et Zabi S. G. F. éditeurs. Editions de l'ORSTOM, Paris, 59-90.

Ekeu-Wei, I. T. (2018). Evaluation of hydrological data collection challenges and flood estimation uncertainties in Nigeria. Environment and Natural Resources Research, 8(2), 44-54.

836 Evtimova, V. V., Donohue, I., 2016. Water-level fluctuations regulate the structure and
837 functioning of natural lakes. Freshwater Biology 61, 251–264.
838 Fish, G.R.,1957. A Seiche Movement and Its Effect on the Hydrology of Lake Victoria.
839 Fish. Publs Colon. Office, London 10, 1-68.
840 Friedrichs, C.T., Aubrey, D.G., 1988. Non-linear tidal distortion in shallow well-mixed
841 estuaries: a synthesis. Estuarine, Coastal and Shelf Science 27 (5), 521-545.
842 Gallo, M.N., Vinzon, S.B., 2005. Generation of overtides and compound tides in Amazon
843 estuary. Ocean Dynamics 55, 441–448.
844 Glenne, B., Simensen, T., 1963. Tidal current choking in the landlocked fjord of
845 NordÅsyatnet. Sarsia, 11(1), 43-73.
846 Gnohossou, P. M., 2006. La faune benthique d'une lagune ouest Africaine (le lac Nokoue
847 au Bénin), diversite, abondance, variations temporelles et spatiales, place dans la
848 chaine trophique. Doctorat, Institut National Polytechnique de Toulouse, France, 184
849 p.
850 Gu, G., Adler, R.F, 2004. Seasonal evolution and variability associated with the West
851 African monsoon system. Journal of Climate 17, 3364– 3377.
852 Guo, L., van der Wegen, M., Jay, D.A., Matte, P., Wang, Z.B., Roelvink, D., He, Q., 2015.
853 River-tide dynamics: Exploration of nonstationary and nonlinear tidal behavior in the
854 Yangtze River estuary. Journal of Geophyical Research Oceans 120, 3499–3521.
855 Guo, L., Wang, Z. B., Townend, I., He, Q., 2019. Quantification of tidal asymmetry and its
856 nonstationary variations. Journal of Geophysical Research: Oceans 124, 773–787.
857 Guragai, B., Hashimoto, T., Oguma, K., Takizawa, S., 2018. Data logger-based
858 measurement of household water consumption and micro-component analysis of an
859 intermittent water supply system. Journal of Cleaner Production 197 (1), 1159-1168.
860 Hill, A.E., 1994. Fortnightly tides in a lagoon with variable choking. Estuar. Coast. Shelf
861 Sci. 38, 423-434.
862 Houéménou, H., Tweed, S., Dobigny, G., Babic, M., Mama, D., Alassane, A., Silmer, R., Ruy,
863 S., Chaigneau, A., Socohou, A., Dossou, H.-J., Badoum, S., Leblanc, M., 2020. Degradation
864 of groundwater quality in expanding cities in West Africa. A case study of the
865 unregulated shallow aquifer in Cotonou. Journal of Hydrology 582, 124438.
866 Hudgins, L., C. A. Friehe, and M. E. Mayer, 1993. Wavelet transforms and atmospheric
867 turbulence. Phys. Rev. Lett., 71, 3279–3282.

868 Huffman, G.J., Bolvin, D.T., Braithwaite, D., Hsu, K., Joyce, R., Xie, P., 2014. NASA Global
869 Precipitation Measurement (GPM) Integrated Multi-Satellite Retrievals for GPM
870 (IMERG) algorithm theoretical basis Doc., version 4.4. NASA GSFC, 30 pp.
871 Jollyman, W.H., 1955. Tides and seiches in lake Nyasa. The Nyasaland Journal, Vol. 8, No.
872 2, 31-35
873 Kjerfve, B., 1986. Comparative oceanography of coastal lagoons. In: Wolfe DA (ed)
874 Estuarine Variability. Academic Press, New York, pp 63–81.
875 Kjerfve, B., Magill, K. E., 1989. Geographic and hydrodynamic characteristics of shallow
876 coastal lagoons. Marine geology, 88(3-4), 187-199.
877 Knoppers, B., 1994. Aquatic primary production in coastal lagoons. In Kjerfve, B. (Ed.).
878 Coastal lagoon processes. Amsterdam, The Netherlands: Elsevier. Elsevier
879 Oceanography Series 60, 243-285.
880 Lalèyè, P., Philippart, J.C., Poncin, P., 1995. Biologie de la reproduction de deux espèces
881 de Chrysichthys (Siluriformes, Bagridae) du lac Nokoue et de la lagune de Porto-Novo
882 au Bénin. Journal of African Zoology 109 (3), 213-224.
883 Lalèyè, P., Niyonkuru, C., Moreau, J., Teugels, G.G., 2003. Spatial and Seasonal
884 Distribution of the Ichthyofauna of Lake Nokoué, Benin, West Africa. African Journal
885 of Aquatic Sciences, 28, 151-161.
886 Lalèyè, P., Villanueva, M.C., Entsua-Mensah, M., Moreau, J., 2007. A review of the aquatic
887 living resources in Gulf of Guinea lagoons with particular emphasis on fisheries
888 management. Journal of Afrotropical Zoology. Proceedings of the Third International
889 Conference on Africa Fish and Fisheries, Cotonou, Benin, 10–14 November 2003,
890 Special issue, 123–136.
891 Lawin, A.E., Hounguè, R., N'Tcha M'Po, Y., Hounguè, N.R., Attogouinon, A., Afouda, A.A.,
892 2019. Mid-Century Climate Change Impacts on Ouémé River Discharge at Bonou
893 Outlet (Benin). Hydrology, 6 (72), https://doi.org/10.3390/hydrology6030072
894 Le Barbé, L., Alé, G., Millet, B., Texier, H., Borel, Y., Gualde, R., 1993. Les ressources en
895 eaux superficielles de la République du Bénin. ORSTOM, Paris, 540 pp.
896 LeBlond, P. H., 1979. Forced fortnightly tides in shallow rivers. Atmosphere-Ocean, 17:3,
897 253-264, doi: 10.1080/07055900.1979.964906
898 Liu, Y., San Liang, X., Weisberg, R. H., 2007. Rectification of the Bias in the Wavelet Power
899 Spectrum. Journal of Atmospheric and Oceanic Technology 24 (12), 2093-2102.

Lobo, M.T.M.P.S., de Souza Nogueira, I., Fabris Sgarbi, L., Nunes Kraus, C., de Oliveira Bomfim, E., Garnier, J., da Motta Marques, D., Bonnet, M.-P., 2018. Morphology-based functional groups as the best tool to characterize shallow lake-dwelling phytoplankton on an Amazonian floodplain. Ecol. Indic. 95, 579–588.

Lyard F., L. Carrere, M. Cancet, A. Guillot, N. Picot, 2021. FES2014, a new finite elements tidal model for global ocean, in preparation, to be submitted to Ocean Sciences-Special issue on Tides.

MacMahan, J., van de Kreeke, J., Reniers, A., Elgar, S., Raubenheimer, B., Thornton, E., Weltmer, M., Rynne, P., Brown, J., 2014. Fortnightly tides and subtidal motions in a choked inlet. Estuarine, Coastal and Shelf Science, 150, 325-331.

Mama, D., Deluchat, V., Bowen, J., Chouti, W., Yao, B., Gnon, B., Baudu, M., 2011. Caractérisation d'un Système Lagunaire en Zone Tropicale: Cas du lac Nokoué (Bénin). Eur. J. Sci. Res. 56 (4), 516–528.

Newton, A., Brito, A.C., Icely, J.D., Derolez, V., Clara, I., Angus, S., Schernewski, G., Inácio, M., Lillebø, A.I., Sousa, A.I., Béjaoui, B., Solidoro, C., Tosic, M., Cañedo-Argüelles, M., Yamamuro, M., Reizopoulou, S., Tseng, H.-C., Canu, D., Roselli, L., Maanan, M., Cristina, S., Ruiz-Fernández, A.C., de Lima, R.F., Kjerfve, B., Rubio-Cisneros, N., Pérez-Ruzafa, A., Marcos, C., Pastres, R., Pranovi, F., Snoussi, M., Turpie, J., Tuchkovenko, Y., Dyack, B., 2018. Assessing, quantifying and valuing the ecosystem services of coastal lagoons. Journal for Nature Conservation 44, 50-65.

N'Tcha M'Po, Y., Lawin, E., Yao, B., Oyerinde, G., Attogouinon, A., Afouda, A., 2017. Decreasing Past and Mid-Century Rainfall Indices over the Ouémé River Basin, Benin (West Africa). Climate 5 (74).

Odountan, O., de Bisthoven, L.J., Koudenoukpo, C., Abou, T., 2019. Spatio-temporal variation of environmental variables and aquatic macroinvertebrate assemblages in Lake Nokoué, a RAMSAR site of Benin. African Journal of Aquatic Science 44 (3), 219–231.

Okpeitcha, V., Chaigneau, A., Morel, Y., Stieglitz, T., Pomalegni, Y., Sohou, Z., Mama, D., 2022. Seasonal and interannual variability of salinity in a large West-African lagoon (Nokoué Lagoon, Benin). Estuarine, Coastal and Shelf Science, 264, 107689.

Omotosho, J.B., 1984. Spatial and seasonal variations of line squalls over West Africa. Arch. Meteorol. Geophys. Bioklimatol. A. 33, 143 – 150.

Omotosho, J.B., 1985. The separate contributions of squall lines, thunderstorms and the monsoon to the total rainfall in Nigeria, J. Clim. 5, 543 – 552.

Percival, D. P., 1995. On estimation of the wavelet variance. Biometrika, 82, 619–631.

Pawlowicz, R., Beardsley, B., Lentz, S., 2002. Classical tidal harmonic analysis including error estimates in MATLAB using T_TIDE. Comput. Geosci. 28, 929–937.

Principaud, J.-M., 1995. La pêche en milieu lagunaire dans le sud-est du Bénin. L'exemple de l'exploitation des acadjas (en danger) sur le lac Nokoué et la basse Sô. In: Cahiers d'outre-mer, 192, 48e année. Togo-Bénin, 519-546.

Pugh, D.T., 1987. Tides, Surges and Mean Sea Level. John Wiley and Sons, New York. 472 pp.

Ray, R. D., 2007. Propagation of the overtide M4 through the deep Atlantic Ocean. Geophyical Research Letters, 34, L21602, doi:10.1029/ 2007GL031618.

Robinson, I.S., Warren, L., Longbottom, J.F., 1983. Sea-level fluctuations in the Fleet, an English tidal lagoon. Estuar. Coast. Shelf Sci. 16, 651-668.

Rydberg, L., Wickbom, L., 1996. Tidal-choking and bed friction in Negombo Lagoon, Sri Lanka. Estuaries 19e3, 540-547.

Schrage, J.M., Fink, A.H., 2007. Use of a rain gauge network to infer the influence of environmental factors on the propagation of quasi-linear convective systems in West Africa. Weather and Forecasting 22, 1016–1030.

Speer, P.E., Aubrey, D.G., Friedrichs, C.T., 1991. Non-linear hydrodynamics of shallow tidal inlet/bay systems. In Tidal Hydrodynamics, edited by B. B. Parker, pp. 321–339, John Wiley, Toronto, Canada.

Sternberg, R. W., 1968. Friction factors in tidal channels with different bed roughness. Marine Geology 6, 243-260.

Stević, F, Mihaljević, M, Špoljarić, D. 2013. Changes of phytoplankton functional groups in a floodplain lake associated with hydrological perturbations. Hydrobiologia 709, 143– 158.

Stieglitz, T. C., van Beek, P., Souhaut, M., and Cook, P. G. 2013. Karstic groundwater discharge and seawater recirculation through sediments in shallow coastal Mediterranean lagoons, determined from water, salt and radon budgets. Marine Chemistry, 156, 73-84.

Stigebrant, A., 1980. Some aspects of tidal interactions with fjord constrictions. Estuar. Coast. Shelf Sci. 11, 151-166.

965 Stigebrandt, A., & Molvær, J. (1988). On the water exchange of Framvaren. Marine
966 Chemistry, 23(3-4), 219-228.
967 Sultan, B., and Janicot, S. 2000: Abrupt shift of the ITCZ over West Africa and intra-
968 seasonal variability. Geophys. Res. Lett. 27, 3353–3356.
969 Texier, H., Colleuil, B., Profizi, J.P., Dossou, C., 1980. Le lac Nokoué, environnement du
970 domaine margino-littoral sud-béninois : bathymétrie, lithofaciès, salinité, mollusque
971 et peuplements végétaux. Bull. Inst. Géol. Bass. Aguit.. Bordeaux 28, 115-142.
972 Torrence, C., Compo, G.P., 1998. A Practical Guide to Wavelet Analysis. Bull. Am. Met. Soc.
973 79, 61-78.
974 Valiela, I., 1995. Marine Ecological Processes, second ed. Springer-Verlag, New York.
975 Varlet, F., 1978. Le régime de la lagune Ébrié, Côte-d'Ivoire. Traits physiques essentiels.
976 Paris, Travaux et Documents essentiels de l'Orstom, 83, 162 pp.
977 Veleda, D., Montagne, R., Araujo, M., 2012. Cross-Wavelet Bias Corrected by Normalizing
978 Scales, Journal of Atmospheric and Oceanic Technology 29 (9), 1401-1408.
979 Ward, P.R.B., 1979. Seiches, tides and wind set-up on Lake Kariba. Limnol. Oceanogr. 24,
980 151-157. 261.
981 Wilson, G.V., Rigby, J.R., Ursic, M., Dabney, S.M., 2016. Soil pipe flow tracer experiments:
982 1. Connectivity and transport characteristics. Hydrology processes 30, 1265-1279.
983 World Bank, 2011. Inondations au Benin: Rapport d'Evaluation des Besoins Post
984 Catastrophe. World Bank: Washington, DC, USA. available at :
985 http://documents1.worldbank.org/curated/en/750141468208769683/pdf/694130
986 ESW0P1240lood0Recovery0Report.pdf (last access: December 24, 2020).
987 Zandagba, J., Moussa, M., Obada, E., Afouda, A., 2016. Hydrodynamic Modeling of Nokoué
988 Lake in Benin. Hydrology 2016, 3, 44.
989